Biochimica et Biophysica Acta 896 (1987) 203–213
Elsevier

BBA 73197

Passive electrical properties of the membrane and cytoplasm of cultured rat basophil leukemia cells. I. Dielectric behavior of cell suspensions in 0.01–500 MHz and its simulation with a single-shell model *

Akihiko Irimajiri, Koji Asami **, Takako Ichinowatari and Yoshito Kinoshita

Department of Physiology, Kochi Medical School, Nankoku, Kochi 781-51 (Japan)

(Received 18 July 1986)

Key words: Dielectric dispersion; Fast impedance analysis; Permittivity; Conductivity; Membrane capacity; Leukemia; (Rat basophil leukemia cell)

Frequency dependence of relative permittivity (dielectric constant) and conductivity, or the 'dielectric dispersion', of cultured cells (RBL-1 line) in suspension was measured using a fast impedance analyzer system capable of scanning 92 frequency points over a 10 kHz–500 MHz range within 80 s. Examination of the resulting dispersion curves of an improved reliability revealed that the dispersions consisted of at least two separate components. The low-frequency component (dispersion 1) had a permittivity increment ($\Delta\varepsilon$) of 10^3–10^4 and a characteristic frequency (f_c) at several hundred kHz; for the high-frequency component (dispersion 2), $\Delta\epsilon$ was smaller by a factor of 10^2 and f_c = 10–30 MHz. Increments $\Delta\varepsilon$ for both components increased with the volume fraction of cell suspension, while f_c did not change appreciably as long as the conductivity of suspending medium was fixed. By fitting a model for shelled spheres (the 'single-shell' model) to the data of dispersion 1, the dielectric capacity of the plasma membrane phase (C_m) was estimated to be approx. 1.4 $\mu F/cm^2$ for the cells in an isotonic medium. However, simulation by this particular shell model failed to reproduce the entire dispersion profile leaving a sizable discrepancy between theory and experiment especially at frequencies above 1 MHz where dispersion 2 took place. This discrepancy could not be filled up even by taking into consideration either the effect of cell size distribution actually determined or that of possible heterogeneity in the intracellular conductivity. The present data strongly indicate the need for a more penetrating model that effectively accounts for the behavior of dispersion 2.

Introduction

The analysis of the dielectric behavior of biological materials has a long history of contribution to our in-depth understanding of the structure and function of biomolecules with the scope of coverage spanning from proteins and nucleic acids down to small molecules like water associated therewith (for reviews, see for example Refs. 1 and 2). At the membrane/cell level and higher, by contrast, the technique of dielectric spectroscopy has received relatively sporadic attention, especially in the last twenty years or so, despite its potential competence to probe noninvasively the electrical structure of living cells and tissues [3,4]. Indeed, the dielectric analysis of suspension systems is much less popular among cell physiologists as compared with the microelectrode technique.

* Dedicated to Professor Akira Inouye on the occasion of his 70th birthday.

** Present address: Institute for Chemical Research, Kyoto University, Uji, Kyoto 611, Japan.

Correspondence: A. Irimajiri, Department of Physiology, Kochi Medical School, Okohcho, Nankoku, Kochi 781-51, Japan.

This rather awkward situation appears to have stemmed from the following facts. (i) Dielectric measurements by conventional type impedance bridges [1,5] take a long time (usually, 20–30 min) to collect one complete set of dispersion data by scanning frequency over e.g. four decades, within which the dielectric dispersions of most cell suspensions conclude. (ii) Without morphological data available, the dispersion data as collected can only report an 'overall' response of a cell suspension, thereby leaving poor resolution with respect to the electrical properties of sub-phases such as cell membrane and organelles. (iii) Even with some structural details in hand, a successful analysis of raw data requires a choice of pertinent models for the suspended phase and, in addition, an accompanying tedium of complicated calculations.

Progress in technology has solved part of the above difficulties by making available several types of precision impedance meters that are rapid enough to operate and can be readily coupled with personal-type computers for both data acquisition and further analysis. The rate determinant would then be a proper choice of models with which the electrical infrastructure of living cells and tissues may be explored to a certain depth. The main theme of the present study dwells on this point.

Recent reports from our laboratory, along the line of approaches based on the 'shell models' [6,7], have dealt with single spherical bilayer membranes as a critical check for the measurement system [8] and thereupon isolated mitochondria [9,10] as an example of the subcellular organelles. In the present series of papers we shall focus on living cells that are to be subjected to the dielectric analysis, by describing the general characteristics of their dispersion behavior in part I, the effects of osmotic perturbation in part II, and morphological correlates for the cell interior in part III followed by a theoretical analysis employing a novel shell model in part IV.

Materials and Methods

Cell culture. Rat leukemic basophilic granulocytes (RBL-1) of unknown passage number, originally obtained from the American Type Culture Collection (Rockville, MD), were a gift from Dr. S. Fujimoto (Department of Immunology, Kochi Medical School). Under a humid atmosphere of 5% CO_2 the cells were grown at 37°C in RPMI 1640 medium (Gibco, Grand Island, NY) containing 4% (v/v) fetal calf serum and 0.1 mg/ml kanamycin, and were fed two to three times per week. For some experiments, sub-cloning was attempted with a view to a better homogeneity in the cell properties, but no difference was observed between the original mixed population and the cloned ones as far as the cells' dielectric behavior and morphology were concerned. No further attempt was made to improve the population homogeneity. Cell viability was routinely checked by a dye exclusion method using 0.04% (w/v) erythrosine B both before and after the dielectric measurements. It was usually better than 90%, and data were discarded when viability was below 80% after the electrical measurements.

Solutions. Two isotonic solutions (A and B) of different ionic strengths were prepared to have the following compositions. Medium A: culture medium (RPMI 1640, Gibco), 10.4 g/l; Hepes-Tris buffer (pH 7.4), 20 mM. Medium B: RPMI 1640, 5.2 g/l; D-mannitol, 112 mM; Hepes-Tris buffer (pH 7.4), 20 mM. Osmolality was determined with a freezing-point depression osmometer, and each medium was adjusted closely to 270 mosmolal. To prepare isosmolal media of different conductivities, the NaCl concentration was varied and the osmolality set slightly hypertonic at 330 ± 4 mosmolal with mannitol. Note that the osmolality, permittivity and conductivity of 'medium' in the Results refer to those of the suspending media separated by centrifugation from cell suspensions after a 15-min equilibration at room temperature.

Dielectric measurements and corrections. Relative permittivities (ε) and conductivities (κ) were measured over a frequency range 10 kHz–500 MHz by an impedance analyzer system as reported by Asami et al. [9]. Briefly, the system consisted of Yokogawa-Hewlett-Packard 4191A and 4192A impedance analyzers, both controlled by a Hewlett-Packard computer model 9825S. Each run of measurements covering 92 frequency points in the log-sweep mode was completed within 80 s. Specifically, the range 1–10 MHz was doubly scanned by both analyzers, and the resulting small differences in raw data were corrected for with respect to the 4192A readings at 1 MHz. A paral-

lel-plate capacitor type measuring cell of a 100-μl volume (cell constant, 0.22 pF) was employed and thermostated at 30°C by circulating deionized water. Raw data from the analyzers were corrected for the series-inductance and stray-capacitance effects by assuming a distributed-parameters network model, as described elsewhere [9].

Morphometry. Immediately after the dielectric measurements, the cells were examined for both viability and morphological integrity, and photographed for morphometry with a differential interference contrast (Nomarski) optics.

Results and Analysis

Reproducibility of dielectric measurements

In general, the use of concentrated, rather than dilute, suspensions is advantageous to reducing artifacts due to electrode polarization. This, however, often exerts deleterious effects on cell integrity, especially when the measurement itself requires a prolonged time to scan over a desired range of frequencies, leading eventually to an adverse temporal variation in the resulting dispersion curves. In order to evaluate whether or not this effect may offer any serious problem to our measurement protocol, we first conducted repeated measurements on both living and killed (i.e., glutaraldehyde-treated) cells confined in the measuring cavity to rather high concentrations.

As time elapsed, the untreated (living) cells showed a decrease in ε and a concurrent increase in κ even with the physiological (culture) medium (Fig. 1A). The rate of change during the initial 12-min period did not exceed 0.15% per min for both ε at 50 kHz and κ at all the frequencies scanned. With the living cells exposed to a half-normal ionic strength (Fig. 1B), on the other hand, temporal changes in the κ-curves became more pronounced (rate, up to 0.5% per min at 10 kHz and 0.35% per min at 100 MHz), while such a 'time effect' was practically negligible with the fixative-treated cells under the same medium condition.

These results indicate that the alterations must have been largely due to changes in the suspension conductivity as a result of net leak of intracellular ions. Despite such inaccuracies inherent in this type of measurements, it was thus demonstrated

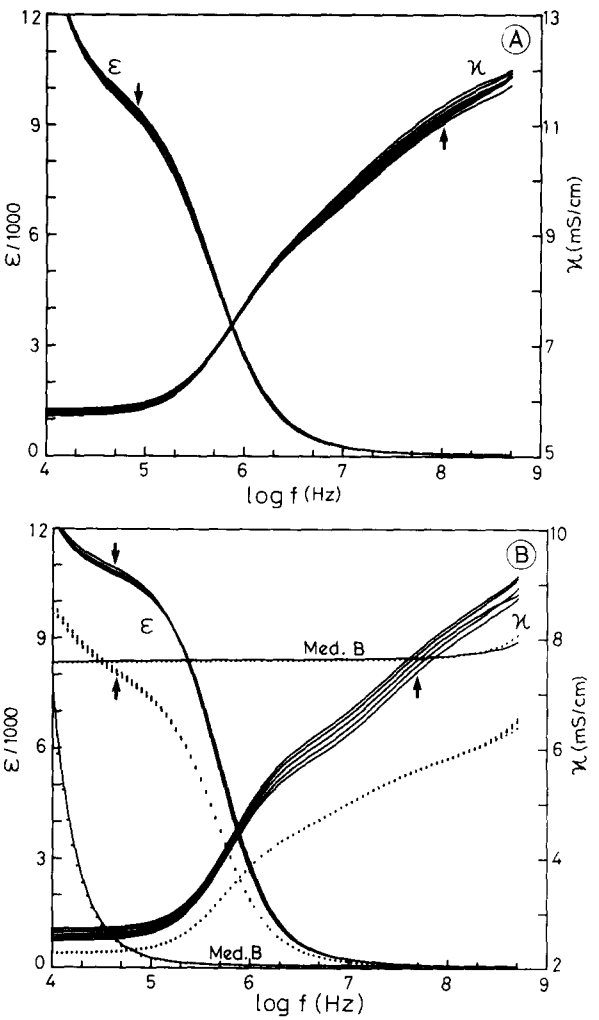

Fig. 1. Successive recordings of the frequency dependence of relative permittivity (ε) and conductivity (κ) for the cells suspended in medium A (A) and medium B (B). Prior to dielectric measurements, the cells were equilibrated with test medium for 10 min at room temperature, loosely packed by centrifugation at 450 × g for 4 min, and gently transferred to the measuring cell by means of a 500-μl Hamilton syringe. Each frequency scan to obtain a single pair of ε- and κ-curves was completed within 80 s, and these scans were repeated at intervals of 4 min. Arrows indicate the up- or downward shift of the dispersion curves during the successive runs. Solid lines, intact cells; dotted lines, glutaraldehyde-fixed cells.

that the frequency scan was rapid enough to override temporal changes in the sample properties as represented by the ε- and κ-curves. Consequently, the whole body of data to be presented below should have reproduced the cells' dielectric behavior in considerable details.

Volume fraction independence of the cell properties

Fig. 2 shows a typical set of dielectric dispersion curves obtained from a single batch of cells successively diluted with medium A. The same data are replotted in complex permittivity and conductivity diagrams (Fig. 3) according to the relations [9]

$$\Delta\varepsilon'' = (\kappa - \kappa_1)/2\pi f\varepsilon_v \quad (1)$$

$$\Delta\kappa'' = 2\pi f\varepsilon_v(\varepsilon - \varepsilon_h) \quad (2)$$

Here, κ_1 is the low-frequency limiting conductivity read from extrapolation in Fig. 3B, ε_h is the high-frequency limiting permittivity taken at the 344-MHz points in Fig. 2A, and ε_v is the absolute permittivity of free space. As seen in the $\Delta\epsilon''$–ε' diagram (Fig. 3A) the degrees of depressed centers (θ) stayed constant at 80.6° irrespective of a wide variation of cell concentrations from 60% to 14%. The corresponding $\Delta\kappa''$–κ' figures (Fig. 3B) resemble each other in their key features of a bimodal pattern, also suggesting a relative constancy of the cells under the imposed test condition.

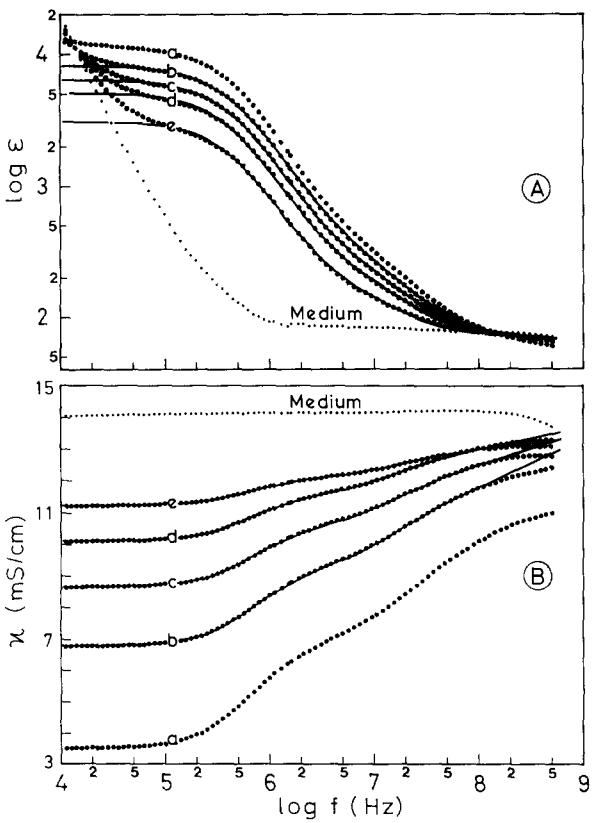

Fig. 2. Dielectric dispersion curves for the cell suspensions equilibrated with medium A and then diluted successively with the same medium. Paired curves marked 'a' refer to the most concentrated (about 60% by volume) suspension and paired curves marked 'e' to the most diluted (about 14% by volume). Solid lines depict the best-fit theoretical curves (for 'a' see Fig. 4) calculated from Eqn. 5 with parameters listed in Table I.

Simulation with a composite Cole-Cole equation

The circular plots in Fig. 3A appear to conform fairly well to the empirical formula of Cole and Cole [11]

$$\epsilon^* = \varepsilon_h + \frac{\Delta\varepsilon}{1 + (jf/f_c)^{\beta}} + \frac{\kappa_1}{j(2\pi f)\varepsilon_v} \quad (3)$$

Here, ε^* is complex relative permittivity and may be written as

$$\varepsilon^* = \varepsilon' - j(\Delta\varepsilon'' + \kappa_1/2\pi f\varepsilon_v), \quad (4)$$

$\Delta\varepsilon$ is permittivity increment ($= \varepsilon_l - \varepsilon_h$), f_c is characteristic frequency at which $\varepsilon = (\Delta\epsilon/2) + \varepsilon_h$, β is a distribution parameter given by $\theta°/90°$, and $j = \sqrt{-1}$. In the complex conductivity plane (Fig.

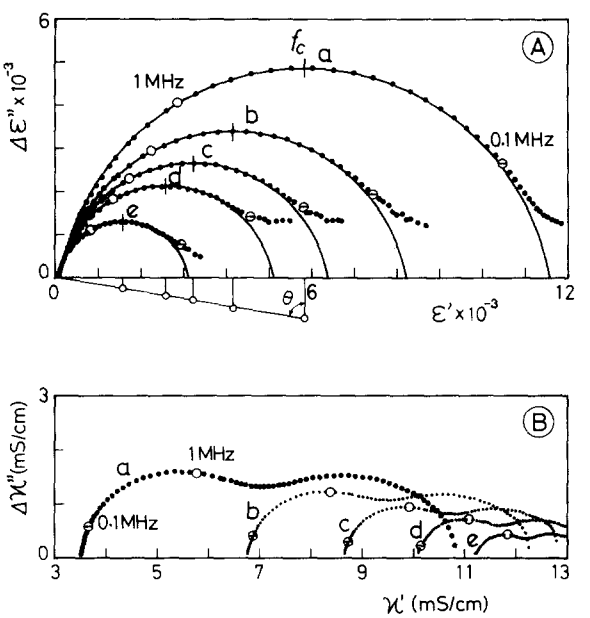

Fig. 3. Complex permittivity (A) and complex conductivity (B) plane plots for data in Fig. 2. Vertical bars in (A) indicate the characteristic frequencies (f_c); open circles below the ε'-axis locate the centers of circular loci.

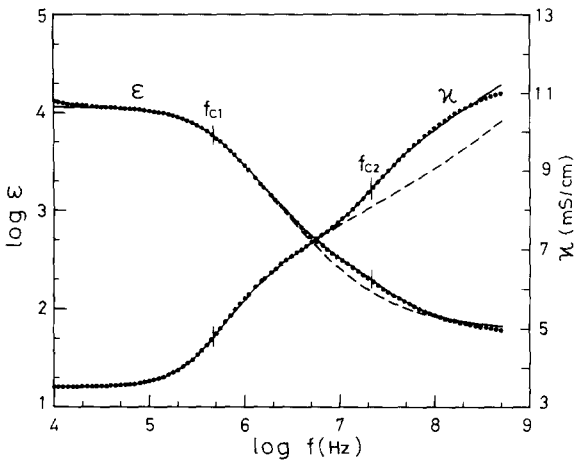

Fig. 4. Simulation of dispersion curves 'a' in Fig. 2. Broken lines are computed from Eqn. 3 and solid lines from Eqn. 5. Values for the parameters involved are listed in Table I (suspension a). Vertical bars, characteristic frequencies for subdispersions 1 and 2.

3B), however, the same data traced a bimodal pattern which was incompatible with the original Cole-Cole formalism of Eqn. 3.

As illustrated in Fig. 4, a much better fit was obtained between theory and experiment by assuming two dispersions of the Cole-Cole type to take place in succession

$$\varepsilon^* = \varepsilon_h + \frac{\Delta\varepsilon_1}{1+(jf/f_{c1})^{\beta_1}} + \frac{\Delta\varepsilon_2}{1+(jf/f_{c2})^{\beta_2}} + \frac{\kappa_1}{j(2\pi f)\varepsilon_v} \qquad (5)$$

where the parameters suffixed 1 and 2 have analogous meanings extended to the two subdispersions. Pertinent numerical results are summarized in Table I, which clearly shows the presence of another smaller dispersion in the 15–20 MHz region. Therefore, the view that single Cole-Cole type relaxation represented by Eqn. 3 might have solely been involved in the present specimen and could accordingly be one promising model for analysis, turned out to be tentative (cf. Fig. 4, broken lines) for simulation of the dielectric behavior of the RBL-1 cells suspended in a physiological medium.

Effect of medium conductivity

Fig. 5 shows dispersion curves for suspensions in which the medium ionic strength was changed

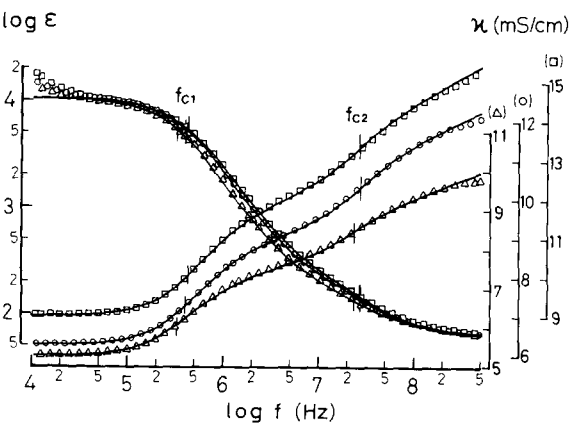

Fig. 5. Dielectric dispersion curves for the cells suspended in three media of different conductivities (κ_a in mS/cm): (□) 18.19, (○) 13.83, and (△) 9.41. Osmolalities were fixed at 330±4 mosmolal by addition of mannitol. Lines depict the best-fit theoretical curves calculated from Eqn. 5 with parameters listed in Table II. f_{c1} and f_{c2}, characteristic frequencies for subdispersions 1 and 2.

TABLE I

PHENOMENOLOGICAL PARAMETERS DETERMINED BY CURVE FITTING FOR DATA IN Figs. 2–4

Volume fractions (Φ) are calculated from the relation: $\Phi = 1-(\kappa_1/\kappa_a)^{2/3}$ where κ_a is medium conductivity (=14.1 mS/cm for this case) and κ_1 suspension conductivity at the low-frequency limit. $\Delta\epsilon$ and f_c are from the circular plots in Fig. 3A; κ_1 taken by extrapolation in Fig. 3B. ε_h, from analyzer readings at 344 MHz. Parameters for subdispersions 1 and 2, determined by fitting Eqn. 5 to data in Figs. 2 and 4.

Suspension	Φ	$\Delta\varepsilon$ ($\times10^{-3}$)	f_c (kHz)	ε_h	$\Delta\varepsilon_1$ ($\times10^{-3}$)	f_{c1} (kHz)	β_1	$\Delta\varepsilon_2$	f_{c2} (MHz)	β_2
a	0.604	11.51	466	63	11.40	463	0.890	115	21	0.95
b	0.388	8.16	498	65	8.07	488	0.875	90	17	0.95
c	0.279	6.34	498	67	6.26	487	0.885	90	17	0.95
d	0.200	5.03	475	70	4.95	470	0.896	77	15	0.95
e	0.142	3.04	481	70	2.99	475	0.900	50	15	0.95

TABLE II

PHENOMENOLOGICAL PARAMETERS DETERMINED BY CURVE FITTING FOR DATA IN Fig. 5

Legend as in Table I.

Medium			Suspension								
Salt concn. (%)	ε_a	κ_a (mS/cm)	κ_1 (mS/cm)	Φ	ε_h	$\Delta\varepsilon_1$ ($\times 10^{-4}$)	f_{c1} (kHz)	β_1	$\Delta\varepsilon_2$	f_{c2} (MHz)	β_2
67	80.7	9.41	5.26	0.321	67	1.010	331	0.898	58	24	0.97
100	81.7	13.83	6.29	0.408	63	1.035	401	0.897	73	27	0.97
133	81.7	18.19	9.02	0.373	64	1.010	434	0.887	68	28	0.99

by $\pm 33\%$ relative to medium A while maintaining the osmolalities at a common value of 330 mosmolal with mannitol. Here again, the gross dispersion profiles appeared bimodal and fitting to Eqn. 5 was excellent, as illustrated in Fig. 5. Values for the parameters thus obtained are listed in Table II. The major effect of increasing medium conductivity was to shift the locations of dispersions 1 and 2 towards the high-frequency side without accompanying notable changes in their dispersion magnitude.

Simulation with the single-shell model

To a first approximation, the cells in free suspension can be regarded as a membraned sphere carrying an aqueous phase (the 'cytoplasm') within it. For a cell so depicted (i.e., the membrane of thickness d and complex permittivity ε_m^* encompasses the core of ε_i^* to make a sphere of radius R), its equivalent homogeneous permittivity $\bar{\varepsilon}_p^*$ is given [12] by

$$\bar{\varepsilon}_p^* = \varepsilon_m^* \frac{2(1-v)\varepsilon_m^* + (1+2v)\varepsilon_i^*}{(2+v)\varepsilon_m^* + (1-v)\varepsilon_i^*} \tag{6}$$

with $v = (1 - d/R)^3$. We designate the above as the 'single-shell' model.

For describing the phenomenon of dielectric dispersion due to these spherical shells in suspension we presently have two theories of different lines: one developed by Pauly and Schwan [13] for relatively dilute suspensions, and the other proposed by Hanai et al. [7] with the aim of extending its applicability to more conncentrated systems. The complex relative permittivity of a suspension of volume fraction Φ is then expressed, according to Pauly and Schwan, as

$$\varepsilon^* = \varepsilon_a^* \frac{2(1-\Phi)\varepsilon_a^* + (1+2\Phi)\bar{\varepsilon}_p^*}{(2+\Phi)\varepsilon_a^* + (1-\Phi)\bar{\varepsilon}_p^*} \tag{7}$$

where ε_a^* is a parameter for the suspending medium. In the theory of Hanai et al., on the other hand, the same is given by the following expression

$$\left(\frac{\varepsilon^* - \bar{\varepsilon}_p^*}{\varepsilon_a^* - \bar{\varepsilon}_p^*}\right)\left(\frac{\varepsilon_a^*}{\varepsilon^*}\right)^{1/3} = 1 - \Phi \tag{8}$$

which is a complex analogue of Bruggeman's equation [14].

On the basis of these theories curve fittings

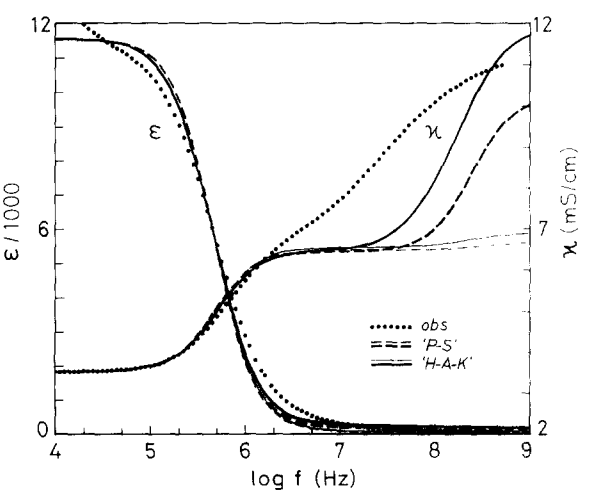

Fig. 6. Simulation of curves 'a' in Fig. 2 (dotted lines) by applying the theory of Pauly and Schwan (broken lines) or that of Hanai et al. (solid lines). Thick and thin lines, respectively, refer to simulations with $\varepsilon_h = 178$ and 63.

TABLE III

PHASE PARAMETERS FOR THE CELLS IN MEDIUM A DETERMINED BY CURVE FITTING WITH A SINGLE-SHELL MODEL

Curve fitting was performed, for data of suspension 'a' in Table I, using the combination of choices: For theory, Pauly-Schwan's ('P-S') or Hanai-Asami-Koizumi's ('H-A-K'); for high-frequency limiting permittivity (ε_h), 63 or 178; and for distribution of cell size, with distribution as in Fig. 7B or without (the simulation curves that resulted are shown in Fig. 6). Other parameters employed are: $\varepsilon_a = 84$, $\kappa_a = 14.14$ mS/cm, $\kappa_m = \kappa_a \times 10^{-7}$, $\varepsilon_i = 11.57 \cdot 10^3$, $\kappa_i = 3.524$ mS/cm, $f_c = 465$ kHz, $R = 6.54$ μm (except for the case of 'H-A-K' with size distribution), and $d = 8$ nm.

Theory	'P-S'		'H-A-K'			
Size distribution	Without		Without		With	
ε_h [a]	63	178	63	178	63	178
Φ	0.668	0.668	0.604	0.604	0.603	0.603
ε_m	16.8	16.8	12.6	12.6	12.7	12.7
ε_i	52.6	200	51.4	279	51.5	280
κ_i (mS/cm)	3.67	3.70	3.26	3.29	3.28	3.31
C_m (μF/cm^2) [b]	1.86	1.86	1.39	1.39	1.40	1.40

[a] Taken as the limiting value for the high-frequency tail of 'P-dispersion' (not of 'Q-dispersion') [6].
[b] Calculated from $C_m = \varepsilon_m \varepsilon_v / d$.

were carried out for a typical experiment as represented by curves 'a' in Fig. 2. The fitting procedures were as described elsewhere [6,7]. The results obtained are shown in Fig. 6 and Table III. It is to be here noted that, in the present case, calculations were made in two ways regarding the choice of values for the phenomenological parameter 'ε_h' which refers to the high-frequency limit of permittivity. In one calculation, we put $\varepsilon_h = 63$, a value immediately read from Table I. As depicted by the thin lines in Fig. 6, simulation for this case resulted in increasing residual values for κ when the frequency was greater than 2 MHz. In the other attempt, a value of 178 was chosen for ε_h, implicating that simulation should be made separately from dispersion 2 whose increment ($\Delta\varepsilon_2$) had been estimated to be 115 (Table I), and hence, that the limiting permittivity for dispersion 1 at its high-frequency tail was to take a sum of $\Delta\varepsilon_2$ and ε_h ($= 63$). The resultant best-fit is traced in thick lines in Fig. 6. Apparently, the fitting with respect to κ at high frequencies improved substantially in the latter trial compared to the former, but a considerable degree of discrepancy still remained between theory and experiment. As a general rule, the relative advantage of Eqn. 8 over Eqn. 7, though still to a limited extent, was nonetheless observed in the simulation of the dielectric behavior of concentrated suspensions.

Assessment of the effects of nonhomogeneity in the cell-associated parameters

As will be detailed in Paper IV, the phenomenological parameters, $\Delta\varepsilon$ and f_c, vary as a function of cell diameter, to name but one among the parameters that define the electrical constitution of a given cell suspension. With the present specimen, the cell shape was almost spherical but the size homogeneity was by no means ideal, as apparent from the size distribution in Fig. 7. Such 'nonhomogeneity' may well cause the dispersion curves to become more or less distorted, so that it was essential to examine to what extent the actual size distribution had been responsible for the observed dispersions. To this end we extended the theory of Hanai et al. (i.e., the combination of Eqns. 6 and 8) to include the case where the suspended phase comprises several subpopulations having different $\tilde{\varepsilon}_p^*$ values, and applied it to plotting the relevant theoretical curves (for procedure see Appendix). In this attempt, computation was made to simulate curves 'a' (Fig. 2) by incorporating a histogram (Fig. 7B) taken immediately after the dielectric measurements. However, no appreciable improvement was embodied in the final curve fittings unless parameters other than the cell diameter were allowed to be distributed (data not shown).

As the second attempt to assess the nonhomo-

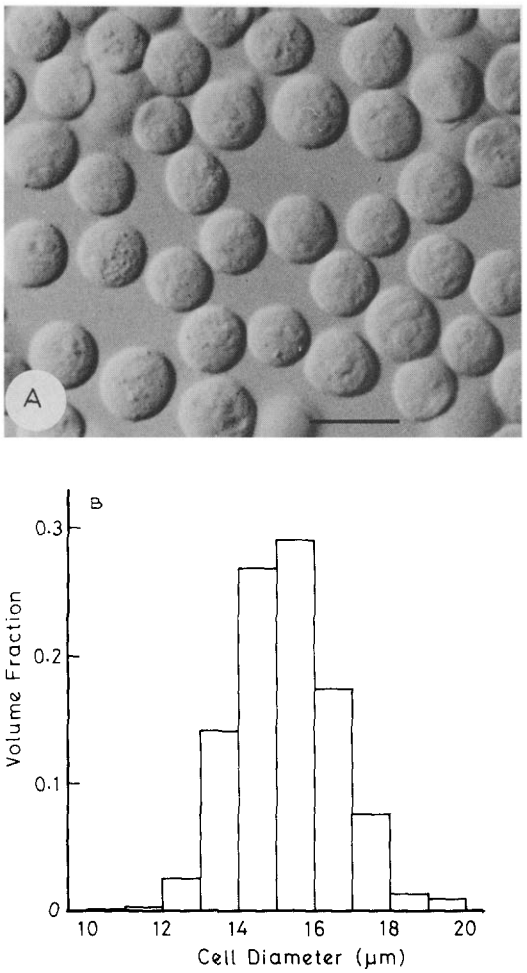

Fig. 7. (A) Differential interference (Nomarski) micrograph of the cells in medium A. Bar, 20 μm. Room temperature. (B) Size distribution. Volume-averaged cell radius R is calculated to be 7.52 ± 0.63 (S.D.) μm ($n = 1007$).

geneity effect, a distribution of κ_i values was assigned to the cell interior, since our experience on synaptosomes [15] indicated that the dispersion broadening was best interpreted in terms of distributed κ_i values among others. For the present case we examined two hypothetical, discrete distributions of κ_i (Fig. 8, inset). The results of these simulations are shown in Fig. 8, in which the values of ε_h were fixed at 178 as before. It was thus demonstrated that the introduction of distributed κ_i values was fairly effective in the fitting of the ε-curve, but that the peculiar behavior of dispersion 2 at high frequencies still remained to be explained.

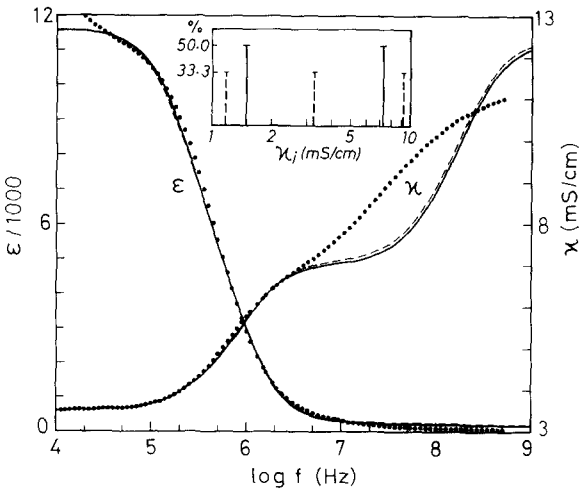

Fig. 8. Simulation of curves 'a' in Fig. 2 (dotted lines) by the theory of Hanai et al. as extended to allow for distributed phase parameters. Solid and broken curves represent calculations for the hypothetical cell populations with, respectively, two and three different κ_i-values as specified in the inset whose ordinates stand for relative volume fraction (in %) of the cells having a given κ_i.

Discussion

Methodology

Results of timed measurements (Fig. 1) demonstrate that the possible artifacts due to temporal variation in the suspension properties were practically negligible and so eventually immaterial to the quality of the presented dispersion data. This fact seems particularly important in that, otherwise, an acceptable quality of dielectric measurements would never have been possible when using living cells suspended to high volume concentrations where a limited supply of oxygen and nutrients should have led to deterioration of the cells quite shortly. In fact, when we measured cultured lymphoma cells with a conventional, manually operated bridge, no fine structure in the resulting dispersion curves could be obtained from the cells exposed to hypotonic stress because of artifacts severely caused by the temporal variation [16].

Also helpful to the measurements was the fact that no sign of separation showed up between cell mass and medium inside the measuring cavity during the course of dielectric measurements. This enabled omission of indifferent, high-density poly-

mers, such as Ficoll and dextran, as an additive that was usually required to prevent the cells from sedimenting [16]. For these reasons the dispersion data presented could be one of the best available from living cells in the sense that they reproduced the cells' dielectric behavior in sufficient details over the frequency range of more than four decades.

Bimodal dispersion profiles

The features of the registered dispersive behavior appear, in the main, to be of the β-dispersion [17], the origin of which is now well known and attributed to frequency-dependent charge accumulation at the membrane/solution interface, or more explicitly, to the membrane capacitance. Similar β-dispersions have been reported for a variety of mammalian cells including erythrocytes (for references, see Schanne and P.-Ceretti [3]), Ehrlich ascites tumor cells [18] and mouse lymphoblasts [16]. Most peculiar to the present specimen are, however, the undulant profiles of κ in the frequency region above a few MHz (Fig. 2B). These undulations resulted in the 'bimodal' pattern in the complex conductivity plots (Fig. 3B), which helped localize dispersion 2 almost two decades distant from dispersion 1, suggesting the existence of an independent dispersive mechanism. This second (minor) dispersion, or the β_1-dispersion according to Schwan [19], could be quantitated through the curve-fitting (Fig. 4) based on Eqn. 5, thereby enabling simulation for the entire frequency dependence of ε^* as a superposition of two Cole-Cole relaxations.

Several mechanisms [1,2,19] may be responsible for the buildup of dispersion 2. First, subcellular organelles, being delimited by their own membranes, are most likely to have caused secondary dispersions of the β-type. These include nuclei, mitochondria, secretory granules and endoplasmic reticulum, and the involvement of the β-type dispersions has been actually confirmed from measurements on isolated organelles in suspension [9,10,20–23]. Secondly, it is conceivable that intracellular macromolecules like proteins and nucleic acids also contributed, at least in part, to the buildup of smaller dispersions in the megahertz region [1,2,19]. Thirdly, the tail of dispersion 2 could be assigned to the δ-dispersion which is due to relaxation of a fraction of water bound to the intracellular macromolecules [1,19].

It might be relavant to point out that no such obviously 'bimodal' patterns were observed in the conductivity dispersion curves for human red blood cells (spherocytes produced by a hypotonic treatment) or mouse lymphoma cells (L5178Y) both examined under the same measurement protocol as that used in the present study (Irimajiri and Asami, unpublished observation). The red cell lacks its internal membranous structures and can be simply regarded as a saccule filled with a rather homogeneous hemoglobin (plus other proteins) solution. By contrast, the lymphoma cell carries a sizable round nuclear mass, and consequently a lesser amount of cytoplasm [16]. The present RBL-1 cell, unlike these two cell species, has an average nuclear fraction of about 30% (v/v) and a greater amount of cytoplasm containing mitochondria, granular inclusions and so on (for morphometric data, see paper III). Therefore, the first argument that a secondary suspension of membrane-covered organelles within the cells gives rise to the major part of dispersion 2 seems highly likely to be the case, although contribution from a variety of possible mechanisms other than this cannot necessarily be excluded.

Limitations of the single-shell model approach

From the results in Figs. 6 and 8 it is concluded that simulation of the present cells' dispersive behavior with the 'single-shell' model is of limited applicability. Discrepancy between theory and experiment, especially in the high-frequency κ-curves, was not effectively accounted for even by taking into consideration the possible effects of either distribution of cell size or heterogeneity in the intracellular conductivity κ_i. On the other hand, the use of a moderately high value for the internal permittivity ε_i ($= 279$) resulted in a closer fit in the simulations than that of $\varepsilon_i = 51$, suggesting here also that a certain mechanism(s) underlying the β-effect was operative inside the cells. It is thus expected that experiment would be better explained by an appropriate modification of the shell model which shall be introduced in Paper IV.

Appendix

Here we outline the procedure for calculating complex permittivity ε^* that represents a concentrated suspension of dielectric particles as an inhomogeneous mixture. A more detailed account will appear separately.

The theory of Hanai [24,25] for concentrated binary dispersion systems (viz., text Eqn. 8) is based on the principle that a series of stepwise additions of particles into a medium of ε_a^* (where a differential addition is made so as to increase volume fraction Φ' by $\Delta\Phi'$) makes a final suspension of volume fraction Φ. The basic assumption in his treatment is such that the process for a small increment in the suspension permittivity ($\Delta\epsilon^*$) due to the differential addition of the suspended phase may be governed by Wagner's mixture equation [26]. So that Hanai's assumption may be written [24] as

$$\frac{2\varepsilon^* + \bar{\varepsilon}_p^*}{3\varepsilon^*(\varepsilon^* - \bar{\varepsilon}_p^*)}\Delta\varepsilon^* = \frac{-\Delta\Phi'}{1-\Phi'} \tag{A1}$$

where $\bar{\varepsilon}_p^*$ denotes equivalent homogeneous permittivity for the suspended particles. For a system of inhomogeneous particles where a subpopulation of particles defined by $\bar{\varepsilon}_{pi}^*$ occupies a fraction f_i (where $\Sigma_i f_i = 1$), the following relation may be assumed

$$\frac{\varepsilon^* - \varepsilon_a^*}{\varepsilon^* + 2\varepsilon_a^*} = \sum_i \frac{\varepsilon\, ay_{pi}^* - \varepsilon_a^*}{\bar{\varepsilon}_{pi}^* + 2\varepsilon_a^*} f_i \Phi \tag{A2}$$

in place of Wagner's mixture equation

$$\frac{\varepsilon^* - \varepsilon_a^*}{\varepsilon^* + 2\varepsilon_a^*} = \frac{\bar{\varepsilon}_p^* - \varepsilon_a^*}{\bar{\varepsilon}_p^* + 2\varepsilon_a^*}\Phi \tag{A3}$$

Then we have, in analogy with Eqn. A1, its extended version:

$$\left(3\varepsilon^* \sum_i \frac{\varepsilon^* - \bar{\varepsilon}_{pi}^*}{2\varepsilon^* + \bar{\varepsilon}_{pi}^*} f_i\right)^{-1} \Delta\varepsilon^* = \frac{-\Delta\Phi'}{1-\Phi'} \tag{A4}$$

Integration of Eqn. A4 over $[\varepsilon_a^*, \varepsilon^*]$ for ε^* and over $[0, \Phi]$ for Φ' should yield an equation for the permittivity of concentrated heterogeneous suspensions. In fact, an analytical expression has been solved for the system of two particle species in mixture [27]; at present, however, it appears almost impossible to solve for the general case. To the case of distributed subpopulations of the present cells, therefore, we had to apply the method of numerical integration of Eqn. A4. Computational errors were within 0.1% for accumulation over 100 sections of $\Delta\Phi'$ and within 0.01% for 1000 sections.

Acknowledgments

We thank Dr. T. Suzaki for reading the manuscript. This work was supported in part by grants 56770052, 56870020 and 60770082 from The Ministry of Education, Science and Culture, Japan.

References

1 Grant, E.H., Sheppard, R.J. and South, G.P. (1978) Dielectric Behaviour of Biological Molecules in Solution. Clarendon Press, Oxford
2 Pethig, R. (1979) Dielectric and Electronic Properties of Biological Materials. John Wiley & Sons, Chichester
3 Schanne, O.F. and P.-Ceretti, E.R. (1978) Impedance Measurements in Biological Cells. John Wiley & Sons, New York
4 Eisenberg, R.S. (1983) in Handbook of Physiology, Skeletal Muscle (Peachey, L.D., ed.), Ch. 11, pp. 301–323, American Physiological Society, Bethesda
5 Schwan, H.P. (1963) in Physical Techniques in Biological Research (Nastuk, W.L., ed.), Vol. 6B, pp. 323–407, Academic Press, New York
6 Hanai, T., Koizumi, N. and Irimajiri, A. (1975) Biophys. Struct. Mech. 1, 285–294
7 Hanai, T., Asami, K. and Koizumi, N. (1979) Bull. Inst. Chem. Res. Kyoto Univ. 57, 297–305
8 Asami, K. and Irimajiri, A. (1984) Biochim. Biophys. Acta 769, 370–376
9 Asami, K., Irimajiri, A., Hanai, T., Shiraishi, N. and Utsumi, K. (1984) Biochim. Biophys. Acta 778, 559–569
10 Asami, K. and Irimajiri, A. (1984) Biochim. Biophys. Acta 778, 570–578
11 Cole, K.S. and Cole, R.H. (1941) J. Chem. Phys. 9, 341–351
12 Irimajiri, A., Hanai, T. and Inouye, A. (1979) J. Theor. Biol. 78, 251–269
13 Pauly, H. and Schwan, H.P. (1959) Z. Naturforsch. 14b, 125–131
14 Bruggeman, D.A.G. (1935) Ann. Phys. 24, 636–664
15 Irimajiri, A., Hanai, T. and Inouye, A. (1975) Biophys. Struct. Mech. 1, 273–283
16 Irimajiri, A., Doida, Y., Hanai, T. and Inouye, A. (1978) J. Membrane Biol. 38, 209–232
17 Schwan, H.P. (1957) Adv. Biol. Med. Phys. 5, 147–209
18 Pauly, H. (1963) Biophysik 1, 143–153

19 Schwan, H.P. (1974) in Biologic Effects and Health Hazards of Microwave Radiation (Czerski, P., ed.), pp. 152–159, Polish Medical Publishers, Warsaw
20 Pauly, H., Packer, L. and Schwan, H.P. (1960) J. Biophys. Biochem. Cytol. 7, 589–601
21 Pauly, H. and Packer, L. (1960) J. Biophys. Biochem. Cytol. 7, 603–612
22 Ogawa, Y., Kurebayashi, N., Irimajiri, A. and Hanai, T. (1981) Adv. Physiol. Sci. 5, 417–435
23 Kuhn, H., Pliquett, F., Wunderlich, S., Schewe, T. and Krause, W. (1983) Biochim. Biophys. Acta 735, 283–290
24 Hanai, T. (1960) Kolloid-Z. 171, 23–31
25 Hanai, T. (1961) Kolloid-Z. 175, 61–62
26 Wagner, K.W. (1914) Arch. Elektrotech. 2, 371–387
27 Hanai, T. and Sekine, K. (1986) Colloid Polymer Sci. 264, 888–895